Desalination and Water Treatment
www.deswater.com

doi: 10.5004/dwt.2020.25004

179 (2020) 332–339
March

Microwave-assisted synthesis of maple-ball-like layered double hydroxides for efficient removal of cationic dye

Xiaohong Wang, Youzhi Tu, Liping Zhu, Lin Wu, Laxia Wu*, Yong Wang, Yebin Guan*

Anhui Key Laboratory of Functional Coordination Compounds, School of Chemistry and Chemical Engineering, Anqing Normal University, Anqing 246011, P.R. China, Tel./Fax:+86-556-5300183; emails: wangxiaohong@aqnu.edu.cn (X.H. Wang), 851048812@qq.com (Y.Z. Tu), 1026856804@qq.com (L.P. Zhu), 46944196@qq.com (L. Wu), wulaxia.1230@163.com (L.X. Wu), 337005942@qq.com (Y. Wang), guanyb@aqnu.edu.cn (Y.B. Guan)

Received 6 September 2018; Accepted 2 October 2019

ABSTRACT

Maple-ball-like Mg–Al layered double hydroxides (LDHs) were successfully prepared via a microwave-assisted heating method in the presence of ethylene glycol water as a solvent, and the synthesis efficiency was significantly improved through the design approach. The product was characterized by a series of techniques, including X-ray diffraction, Fourier transforms infrared spectroscopy, field emission scanning electron microscopy, thermogravimetric analysis, and Brunauer–Emmett–Teller. The as-synthesized Mg–Al LDHs display considerable adsorption performance for the cationic dye methylene orange from aqueous solution within extremely short processing time. This study offers a low-cost approach for the synthesis of an Mg–Al LDH material that could be used as an effective adsorbent for the removal of dyes from wastewater.

Keywords: Mg–Al LDHs; Microwave; Adsorption; Dyes

1. Introduction

Large amounts of different types of dye are synthesized every year and are widely used in various fields, including cosmetics, textiles, leather, pharmaceuticals, food, etc. [1]. Although these dyes have brought us a colorful world, they have also brought many contaminants causing severe water pollution. In particular, dyes derived from the printing and textile industry wastewater are generally toxic and have had a tremendous influence on aqueous ecosystems in China over the last decades [2]. Due to the hazardous nature and low biodegradability of dyes, a number of techniques have been developed, including photodegradation [3], advanced oxidation processes [4], biodegradation [5] and adsorption [6], to remove dyes from aqueous solutions. Among these technologies, adsorption methods have been adopted as one of the potential methods due to their simplicity, efficiency, and lower cost [6–10]. In particular, adsorbents with abundant active sites play a crucial role in the factors affecting adsorption performance. Among the diverse adsorbents, layered double hydroxides (LDHs) have been shown to have high adsorption properties for dye removal since they have a high specific surface area, non-toxicity and ion-exchange capability [11–13].

LDHs are a group of inorganic layered materials in which the trivalent cations substituted for the divalent layer cations partially result in positively charged hydroxide layers and hydrated anions located in the interlayer gallery provide charge balance [14–16]. Therefore, LDH chemical composition can be represented by the formula $[M^{2+}_{1-y}M^{3+}_{y}(OH)_2]^{y+}(A^{n-})_{y/n}\cdot zH_2O$ (M^{2+}, M^{3+} and A^{n-} represent the bivalent cations, trivalent cations and anions, respectively, and y is usually $0.2 < y < 0.33$) [17–19]. Their particular interlayer and functional surface properties can endow LDHs with a high ability to exchange or form strong surface complexes with various organic dyes in aqueous solutions [20,21].

* Corresponding authors.

1944-3994/1944-3986 © 2020 Desalination Publications. All rights reserved.

In the past decade, a variety of methods, such as co-precipitation [22], hydrolysis [23], sol-gel treatment [24], microwave-assisted structure reconstruction [25], hydrothermal treatment [26], sonication [27], spray drying [28], and mechanochemistry [29], have been applied for the fabrication of LDH materials. Among them, the use of microwave-assisted heating as a potential method for the preparation of LDH materials has received widespread attention because of its advantages of rapid heating, a smaller thermal gradient, environmental friendliness, and low cost compared with other conventional fabrication processes, etc. [30–32]. In this study, a microwave-assisted heating method was adopted to prepare Mg–Al LDHs by using ethylene glycol (EG) and a water solvent, and the addition of EG improved the synthesis efficiency because of the higher microwave absorption properties of EG. Maple-ball-like as-synthesized Mg–Al LDHs were obtained with considerable adsorption properties for the cationic dye methylene orange (MO) in aqueous solution. A possible adsorption mechanism between LDH particles and dye molecules was also proposed.

2. Experimental section

2.1. Mg–Al LDHs preparation

Magnesium chloride hexahydrate ($MgCl_2{\cdot}6H_2O$) and EG (EG, M_W = 62.07) were purchased from Sinopharm Chemical Reagent Co. Ltd., (Shanghai, China). Aluminum nitrate hexahydrate ($AlCl_3{\cdot}6H_2O$) and sodium hydroxide (NaOH) were purchased from Shanghai Aladdin Biochemical Technology Co. Ltd. Deionized water (18.25 MΩ cm) was used throughout all experiments.

The Mg–Al LDH material was synthesized via a microwave heating method with a molar ratio of Mg^{2+}:Al^{3+} = 2:1. Typically, 0.1 mol of $MgCl_2{\cdot}6H_2O$, 0.05 mol of $AlCl_3{\cdot}6H_2O$ and 0.2 mol of NaOH were dissolved in a 75 mL aqueous solution, and then the solution was transferred into a 250 mL round-bottomed flask. Afterward, 25 mL of EG was added to the flask and mixed with shaking. Then, the flask was quickly placed in a microwave reaction device and heated at 300 W (2.45×10^9 Hz working frequency, power density 10 mW cm^{-2}) and maintained for 30 min. After natural cooling to room temperature, the white precipitate was retrieved by filtration, washed three times with deionized water and then dried at 60°C for 24 h.

2.2. Characterization of LDHs

X-ray diffraction (XRD) patterns of the sample were recorded using a SHIMADZU XRD-6000 X-ray diffractometer (Kyoto, Japan) with Cu kα radiation (λ = 1.5406 Å) at 40 kV and 20 mA. Fourier transform infrared (FT-IR) spectra were recorded on a Nicolet iS 50 attenuated total reflection instrument (Massachusetts, USA) over the range of 400–4,000 cm^{-1} by using the KBr pellet technique. The morphologies of the LDHs were characterized by using scanning electron microscopy (SEM) (Hitachi SU-8010, Tokyo, Japan). The pore structure of the LDH samples was analyzed by nitrogen adsorption–desorption at 77 K on a BEL MAX surface area analyzer (Osaka, Japan). The surface area was evaluated by the Brunauer–Emmett–Teller model, and the pore size distribution was estimated via the Barrett–Joyner–Halenda theory. Thermogravimetric analysis (TGA) data were collected from a thermogravimetric analyzer instrument (STA 409 PC, Netzsch, Bavaria, Germany) under nitrogen flow, and the temperature ranged from room temperature to 800°C with a heating rate of 10°C min^{-1}. A PerkinElmer Lambda 950 UV-Vis spectrum spectrophotometer (Massachusetts, USA) was used to measure the concentration of the dye.

2.3. Adsorption experiments

MO adsorption experiments were carried out by varying the reaction conditions, including the contact time, initial concentration of MO, pH and adsorption temperature. For each test, only one parameter was varied while the others were kept constant. The MO absorption capacity of (Q_t, mg g^{-1}) and removal rate (R%) for each experiment were calculated using the following equations:

$$Q_t = \frac{\left(C_0 - C_t\right)V}{m} \tag{1}$$

$$R\% = \frac{C_0 - C_e}{C_0} \times 100\% \tag{2}$$

where C_0 and C_t are the dye concentration at the initial time and the given time t (min), respectively, V is the volume of dye solution, m is the weight of absorbent, and C_e is the equilibrium concentration.

3. Results and discussion

3.1. Characterization of Mg–Al LDHs

The XRD patterns of the samples containing Mg–Al LDHs as the major phase are displayed in Fig. 1. Comparing the standard reference pattern of simulated Mg–Al LDHs (JCPDS no. 35–0965, Fig. 1a) and that of the synthesized Mg–Al LDH sample reveals that the peaks corresponding to (003), (006), (012), (015), and (110) are the characteristic peaks of the Mg–Al LDH material in the synthesized sample (Fig. 1b). Moreover, the wideness of the peaks indicates the small crystallite size of the LDH particles, and the symmetric peaks of the (003) and (006) planes at lower 2θ angles represent the stacking order of layers in the Mg–Al LDHs. The interlayer spacing (d) of 7.71 Å was calculated from the characteristic (003) plane at a 2θ of 11.47° [33]. When only water was used as the solvent, the intensity of the peaks of (003) and (006) decreased slightly, indicating the high crystallinity of the LDHs obtained from the EG/water solution.

The FT-IR spectra of the Mg–Al LDHs are shown in Fig. 2. The strong and broad absorption band at 3,468 cm^{-1} can be attributed to the O–H stretching vibration of surface and/or interlayer water molecules. In addition, the band at 1,642 cm^{-1} is ascribed to the O–H bending vibration of water molecules [34]. The absorption band at 1,398 cm^{-1} is the characteristic asymmetrical stretching vibration of CO_3^{2-}, which may result from the dissolved CO_2 in solution [35]. The broad peak at approximately 624 cm^{-1} is from the O–H vibration of the hydroxide layer [36].

Fig. 3 shows typical field emission scanning electron microscopy images of the as-prepared Mg–Al LDHs. The spherical-like morphology of the Mg–Al LDHs can be seen in the low-magnification SEM image (Fig. 3a); however, the Mg–Al LDH spheres are composed of non-uniform globules with a size distribution between 0.5 and 1.0 μm in the high-magnification SEM image (Fig. 3b). Interestingly, the surface of these globules consists of nanometric building blocks, and these ultrathin platelets are interconnected to each other to self-assemble into maple-ball-like hierarchical structures without sticking together. However, if no EG molecules were added to the solution, only some irregular aggregated particles were obtained (Figs. 3c and d), which indicates that EG molecules enhanced the maple-ball-like LDH particle formation. This kind of maple-ball-like morphology of Mg–Al LDHs is different from those obtained

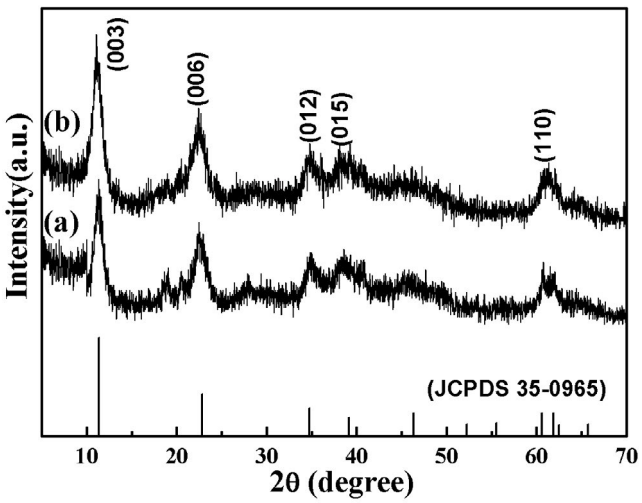

Fig. 1. X-ray diffraction patterns of simulated and Mg–Al LDH obtained from water (a) and EG/water solution (b).

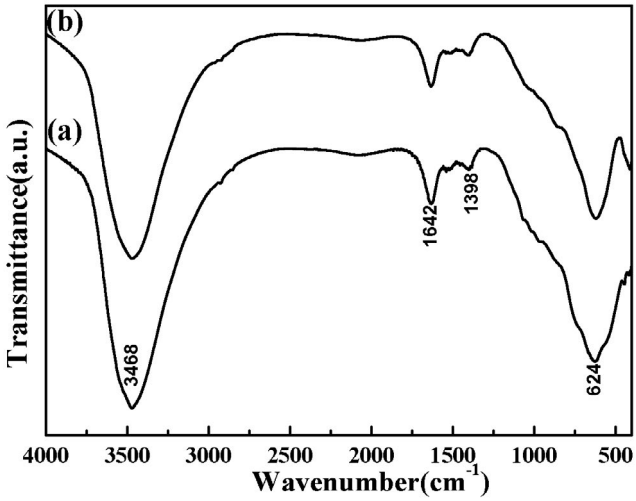

Fig. 2. FT-IR spectra of Mg–Al LDHs particles obtained from water (a) and EG/water solution (b).

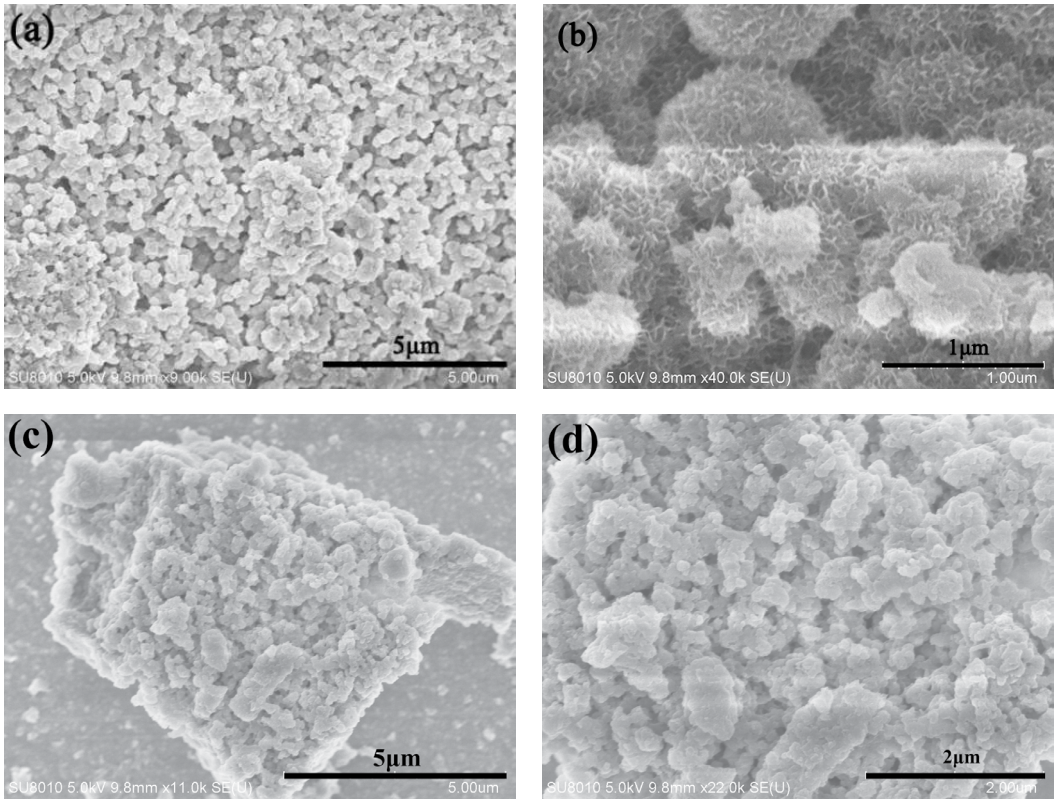

Fig. 3. FESEM images of the Mg–Al LDHs particles obtained from EG/water solution (a,b) and water (c,d).

by hydrothermal synthesis and coprecipitation methods, which exhibit globular aggregates [37], bead-like fine particle aggregates [38], and hexagonal platelets [39]. EG molecules are small and can form hydrogen-bonded networks similar in nature to those of water but possess larger a tangent loss than H_2O molecules. Microwave radiation can lead to a high heating rate via dielectric loss during the nucleation process [40], which is important for fast nucleation and crystal growth and has also widely facilitated the formation of better-dispersed and size-tailored crystals [41,42]. In this work, microwave irradiation probably enhanced the interactions between the EG molecules and the Mg–Al LDH nuclei. In pure water, driven by the hydrophobic effect, the nuclei aggregate together and further grow into microspheres via oriented attachment growth [34]. In contrast, in EG/water solution, the hydrogen bonding between the Mg–Al LDH nuclei and the hydroxyl groups on EG molecules results in the enrichment of EG around Mg–Al LDHs, which tends to inhibit the aggregation of the Mg–Al LDH nuclei and leads to the formation of 2-dimensional platelets after oriented attachment [43], which ultimately results in the formation of a Mg–Al LDH maple-ball-like morphology.

The surface area, pore volume and average pore diameter of the Mg–Al LDH maple-like balls are 67.56 $m^2\ g^{-1}$, 15.52 $cm^3\ g^{-1}$, and 4.21 nm, respectively. The N_2 adsorption–desorption isotherm of the Mg–Al LDHs is shown in Fig. 4. The isotherm can be classified as a type IV curve according to the International Union of Pure and Applied Chemistry classification because of the typical H3 hysteresis loop at high relative pressure, which indicates that the plate-like particle aggregation led to the formation of pores and the mesoporosity of the Mg–Al LDHs. It is expected that this LDH material can be used as a potential adsorbent.

The stability of the Mg–Al LDH samples under continuous heating was investigated using TGA. As shown in Fig. 5, there are three main consecutive weight loss stages at the given heating rate of 10°C min^{-1}. In detail, the weight loss of 14.2% from 25°C to 230°C involves the release of the physically adsorbed water both on the surface and in the layers of LDHs [42]. The second mass loss stage observed between 230°C and 430°C is approximately 23.5%, corresponding to water molecule removal by a dehydroxylation process [41]. The last mass loss step happened from 430°C to 800°C, and the approximately 4.8% mass loss is probably because of the removal of interlayer carbonate species [42].

3.2. Adsorption performance of Mg–Al LDHs

The adsorption performance of the as-prepared Mg–Al LDHs for organic cationic dyes was studied by performing adsorption experiments with MO. The concentration of MO was determined by observing the change in UV-visible spectra. Fig. 6 shows the relationship between the removal rate of MO and the solution pH value at an initial MO concentration of 100 ppm. The removal ratio of MO increased with pH in the range of 4 to 8 but decreased with pH in the range of 9–12, and the maximum adsorption capacity and removal ratio reached 167.82 mg g^{-1} and 85.0%, respectively, at pH = 8. The solution pH remarkably affects the adsorption behavior at the water-absorbent interface, and this effect can be represented by the point of zero charge (pHpzc), an important parameter for determining the surface charge of an adsorbent. If the pH is lower than the pHpzc, the positive surface charge of the adsorbent will facilitate electrostatic interactions between the adsorbent and MO. It has been reported that the pHpzc value of Mg–Al LDHs is between 6.8 and 8.9 [44], so the electrostatic attraction between the sulfonate groups of MO and the active sites of the absorbent at pH 4.0–8.0 is increased, which promotes the adsorption capacity of the dye. If the pH value is greater than 9.0, the electrostatic interactions between the MO dye molecules and LDHs will be reduced due to the competitive behavior between OH– ions and MO for adsorption onto Mg–Al LDHs. Therefore, an optimum pH value of 8 for testing the adsorption performance of the Mg–Al LDH absorbent was adopted in follow-up experiments. However, the maximum adsorption capacity and removal ratio of particles from water only reached 65.36 mg g^{-1} and 33.1%, respectively. This result indicates that the mesoporous structure of the maple-ball-like Mg–Al LDHs effectively increased the adsorption capacity.

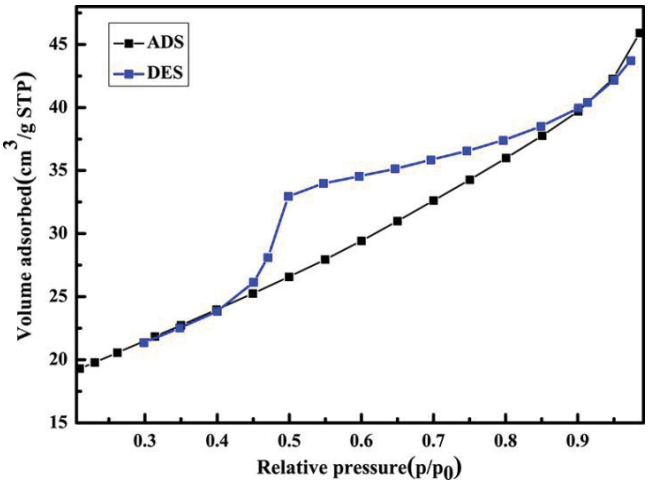

Fig. 4. N_2 adsorption/desorption isotherms of maple-ball like Mg–Al LDHs.

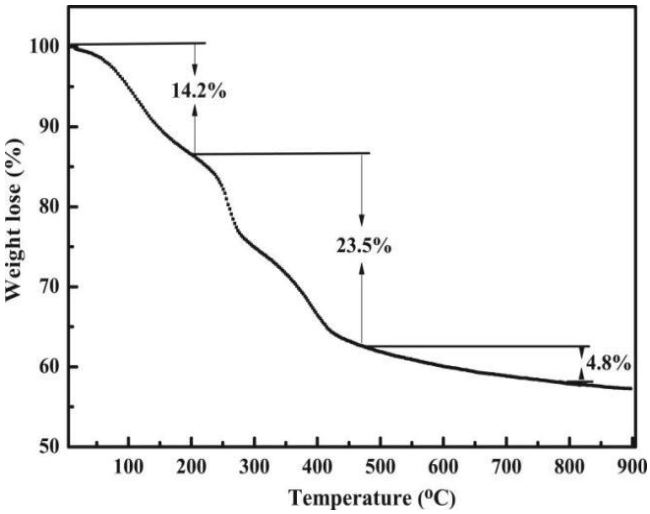

Fig. 5. TGA curve of maple-ball like Mg–Al LDHs.

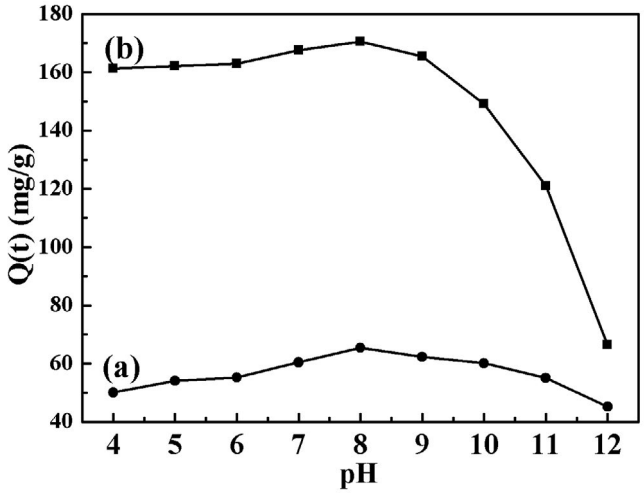

Fig. 6. Effect of solution pH on adsorption capacity of MO onto the Mg–Al LDH obtained from water (a) and EG/water solution (b).

In general, Mg–Al LDHs are anionic minerals [45] and are thus potential adsorbents for removing dyes from wastewater. For cationic MO molecules, the electrostatic attraction between the surface of the Mg–Al LDHs and MO molecules is an important factor influencing the adsorption performance [46–48]. Moreover, materials possessing hierarchically porous structures and large specific surface areas possibly provide more efficient transport pathways and available active adsorption sites to improve adsorption performance [49,50]. Compared with the aggregated Mg–Al LDH particles obtained from water solution, the mesoporous hierarchical maple-like Mg–Al LDH balls without stacking are composed of interconnected nanosheets with a higher surface area and can provide more active adsorption sites, which are conducive to the fast transport of MO dyes in interconnected pore structure systems, thus enhancing the adsorption capacity [45].

Fig. 7 demonstrates the effect of the initial dye concentration (i.e., 20, 40, 60, 80, 100, 120, 150, and 200 ppm) on the amount adsorbed onto 500 ppm Mg–Al LDHs at pH = 8.0. As shown in Fig. 7a, the adsorption capacity increased as the initial dye concentration increased at a fixed adsorbent dose since the interaction between higher ionic concentrations of MO and the adsorbent was stronger. Fig. 7b reveals that the removal efficiency reached 100% at a lower dye initial concentration (20, 40, and 60 ppm) and the removal efficiency decreased to 85.3% when the MO initial dye concentration increased to 200 ppm. The adsorption rate of MO is very fast, and the adsorption equilibrium was reached within 5 min. This rapid adsorption rate can be ascribed to the availability of more active adsorption sites on the surface of the Mg–Al LDHs upon initial contact.

For practical applications, the stability and reusability of adsorbents are greatly important, so a cycling experiment was further carried out with the Mg–Al LDHs. The concentrations of adsorbent and MO used in the experiments were 200 and 500 ppm (50 mL), respectively. After the first 50 min of adsorption, the Mg–Al LDH adsorbent was recovered, washed with 1 mol L^{-1} NaOH solution, and re-dispersed in

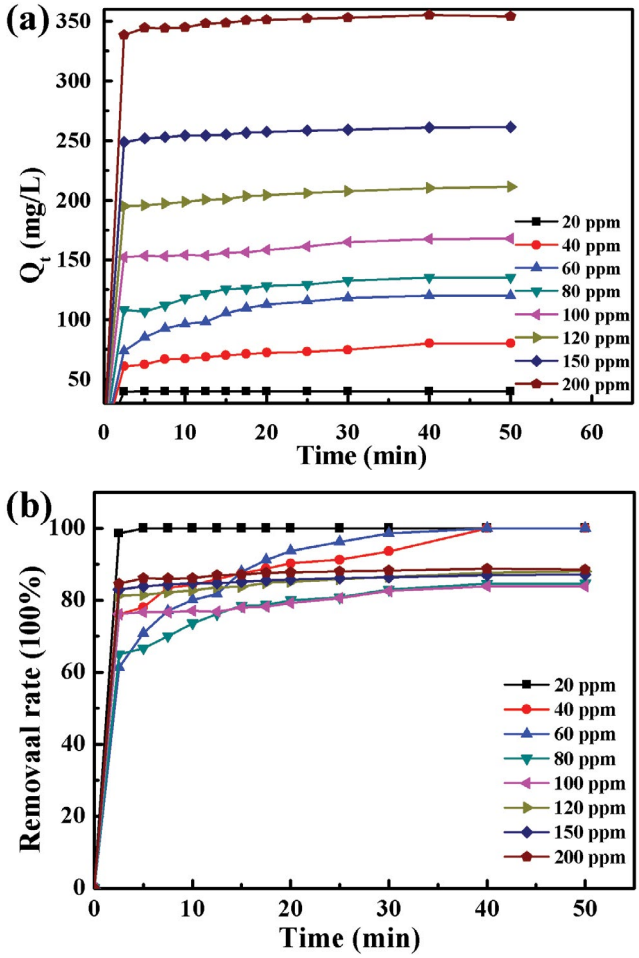

Fig. 7. Effect of initial dye concentration on adsorption capacity (a) and removal efficiency (b) of MO on maple-ball like Mg–Al LDHs.

MO dye solution for the next run. The MO removal rates were 85.3%, 82.1%, 79.5%, 75.8%, and 73.4% for the first to fifth runs (Fig. 8). The removal efficiency of Mg–Al LDHs for MO dye was reduced by 10.9% after five successive runs. This decrease during the repeated runs is probably ascribed to the consumption of the Mg–Al LDH adsorbent during the recovery and redispersion process.

Adsorption kinetic studies were further carried out to investigate the pivotal step that governs the overall removal efficiency of the adsorption process. Pseudo-first and pseudo-second-order kinetic models were applied to fit the experimental data, as described in the following equations [51]:

$$\log\left(Q_e - Q_t\right) = \ln Q_e \frac{-k_1 t}{2.303} \tag{3}$$

$$\frac{t}{Q_t} = \frac{1}{k_2 Q_e^2} + \frac{t}{Q_e} \tag{4}$$

where Q_e and Q_t are the adsorption capacity (mg g^{-1}) of Mg–Al at equilibrium and time t, respectively, and k_1 (min^{-1}) and k_2

(g mg^{-1} min^{-1}) are the equilibrium rate constants of pseudo-first and pseudo-second-order adsorption, respectively. A comparison of pseudo-first and pseudo-second-order model parameters, calculated $Q_{e,cal}$ values and experimental $Q_{e,exp}$ values is summarized in Table 1, and a linear plot of t/Q_t vs. time t is given in Fig. 9. The pseudo-second-order kinetic model fits better according to the correlation coefficient (R^2), while the $Q_{e,cal}$ calculated by the pseudo-second-order model is much closer to the experimental $Q_{e,exp}$. Therefore, it is considered that the adsorption rate-determining step is chemical adsorption involving electrostatic interactions between the MO molecules and Mg–Al LDHs.

Temperature also affects the adsorption process [52]. The temperature effect on MO dye adsorption behavior was evaluated at 298, 308, 318 and 328 K. Three basic thermodynamic parameters, including the changes in the standard enthalpy ($\Delta H°$), the standard Gibbs free energy ($\Delta G°$) and the standard entropy ($\Delta S°$), were calculated using the following equations:

$$k_d = \frac{Q_t}{C_e} \tag{5}$$

$$\Delta G° = RT \ln k_d \tag{6}$$

$$\ln k_d = \frac{\Delta S°}{R} \frac{-\Delta H°}{RT} \tag{7}$$

where k_d (L g^{-1}) is the distribution coefficient, T (K) is the system temperature and R (8.314 J mol^{-1} K^{-1}) is the universal gas constant. The values of $\Delta H°$ and $\Delta S°$ were calculated

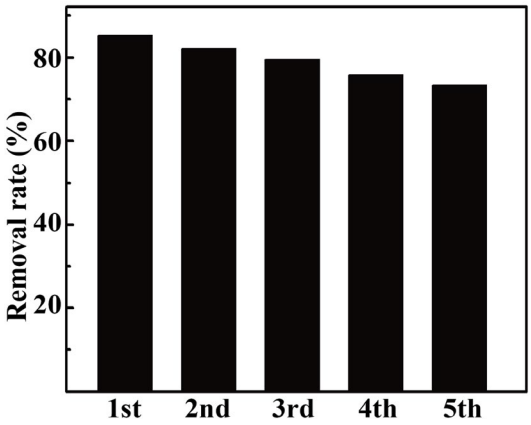

Fig. 8. Cycling runs for dye removal efficiency of MO on maple-ball like Mg–Al LDHs.

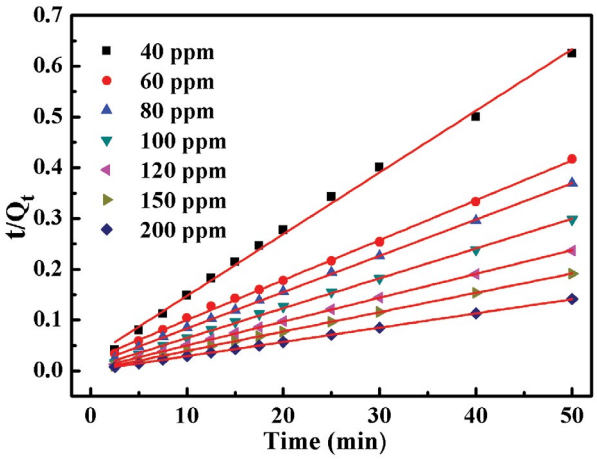

Fig. 9. Adsorption kinetics fitting of pseudo-second-order on maple-ball like Mg–Al LDHs.

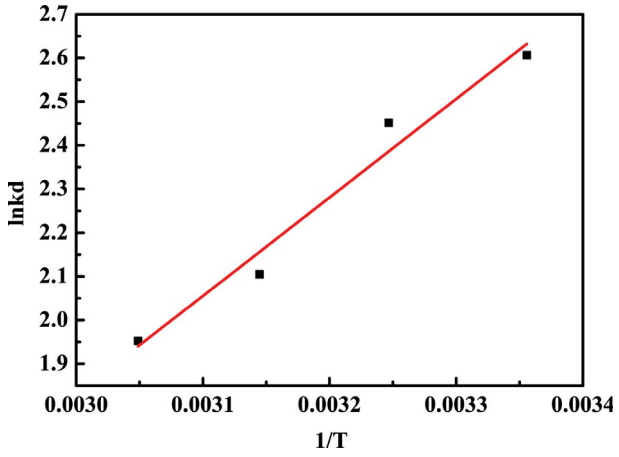

Fig. 10. Effects of temperature on Mg–Al LDHs adsorption process.

Table 1
Kinetics parameters of the adsorption

		First-order parameter			Second-order parameter		
C_0 (mg L^{-1})	$Q_{e,exp}$ (mg L^{-1})	$Q_{e,cal}$ (mg L^{-1})	k_1 (min^{-1})	R^2	$Q_{e,cal}$ (mg L^{-1})	$k_2 \times 10^3$ (g mg^{-1} min^{-1})	R^2
40	80.00	20.44	0.0462	0.9798	82.30	0.1476	0.9969
60	120.00	70.72	0.1138	0.9729	127.23	0.0618	0.9987
80	135.45	66.65	0.1261	0.8741	139.66	0.0512	0.9991
100	167.82	42.89	0.1082	0.7263	170.36	0.0345	0.9998
120	211.38	24.36	0.0681	0.9472	213.22	0.0220	0.9999
150	261.39	17.52	0.0808	0.9232	262.47	0.0145	0.9999
200	354.10	15.61	0.0605	0.9444	355.87	0.0079	0.9995

Table 2
Thermodynamic parameters of adsorption

T (K)	$\Delta G°$ (KJ mol^{-1})	$\Delta H°$ (KJ mol^{-1})	$\Delta S°$ (J mol^{-1} k^{-1})	Removal efficiency (%)
298	–6.466	–18.837	41.05	87.14%
308	–6.274			85.29%
318	–5.563			80.40%
328	–5.323			77.88%

by using the van't Hoff equation, and all the thermodynamic parameters are listed in Table 2. The van't Hoff plots for the adsorption of MO onto the Mg–Al LDHs are shown in Fig. 10. The negative values of $\Delta G°$ under different conditions indicate the spontaneous adsorption process of MO on the Mg–Al LDHs. The value of $\Delta G°$ increased from –6.466 to –5.323 KJ mol^{-1}, and the removal efficiency decreased with temperature, indicating that adsorption is more favorable at low temperatures. The negative value of $\Delta H°$ indicates that the adsorption process is exothermic and more favorable as the temperature decreases [47]. Moreover, the positive value of $\Delta S°$ indicates that the adsorption of MO onto the Mg–Al LDHs results in a randomness decrease at the solid–liquid interface [53].

4. Conclusions

Maple-ball like Mg–Al LDHs were rapidly prepared via a simple microwave-assisted synthesis method that can be applied for the removal of cationic dye MO from aqueous solution. The N_2 adsorption–desorption results show that the Mg–Al LDHs are predominantly mesoporous. The adsorption process of MO quickly reached equilibrium within 5 min, and the experimental kinetic data are in good agreement with the pseudo-second-order kinetic model. The adsorption of MO onto Mg–Al LDHs is pH-dependent and decreases as the temperature increases from 298 to 328 K. This simple synthesis method and the spontaneous and rapid adsorption of cationic dye ensure that this kind of Mg–Al LDH material could be applied as an effective adsorbent for the removal of dye from wastewater.

Acknowledgments

This research was financially supported by the National Natural Science Foundation of China (No. 41402037, 51672001) and University Natural Science Research Project of Anhui Province (CN) (No. KJ2018A0378, KJ2019A0577).

References

[1] M.T. Yagub, T.K. Sen, S. Afroze, H.M. Ang, Dye and its removal from aqueous solution by adsorption: a review, Adv. Colloid Interface Sci., 209 (2014) 172–184.
[2] J.H. Qu, M.H. Fan, The current state of water quality and technology development for water pollution control in China, Crit. Rev. Env. Sci. Technol., 40 (2010) 519–560.
[3] S. Zargari, R. Rahimi, A. Ghaffarinejad, A. Morsali, Enhanced visible light photocurrent response and photodegradation efficiency over TiO_2–graphene nanocomposite pillared with tin porphyrin, J. Colloid Interface Sci., 466 (2016) 310–321.
[4] S. Cotillas, J. Llanos, P. Cañizares, D. Clematis, G. Cerisola, M.A. Rodrigo, M. Panizza, Removal of Procion Red MX-5B dye from wastewater by conductive-diamond electrochemical oxidation, Electrochim. Acta, 263 (2018) 1–7.
[5] J. Fan, D. Chen, N. Li, Q. Xu, H. Li, J. He, J. Lu, Adsorption and biodegradation of dye in wastewater with Fe_3O_4@MIL-100 (Fe) core-shell bio-nanocomposites, Chemosphere, 191 (2018) 315–323.
[6] K. Wang, J. Fu, S. Wang, M. Gao, J. Zhu, Z. Wang, Q. Xu, Polydopamine-coated magnetic nanochains as efficient dye adsorbent with good recyclability and magnetic separability, J. Colloid Interface Sci., 516 (2018) 263–273.
[7] M.-X. Zhu, L. Lee, H.-H. Wang, Z. Wang, Removal of an anionic dye by adsorption/precipitation processes using alkaline white mud, J. Hazard. Mater., 149 (2007) 735–741.
[8] M. Vakili, M. Rafatullah, B. Salamatinia, A.Z. Abdullah, M.H. Ibrahim, K.B. Tan, Z. Gholami, P. Amouzgar, Application of chitosan and its derivatives as adsorbents for dye removal from water and wastewater: a review, Carbohydr. Polym., 113 (2014) 115–130.
[9] J.-S. Qin, S.-R. Zhang, D.-Y. Du, P. Shen, S.-J. Bao, Y.-Q. Lan, Z.-M. Su, A microporous anionic metal–organic framework for sensing luminescence of Lanthanide(III) ions and selective absorption of dyes by ionic exchange, Chem. Eur. J., 20 (2014) 5625–5630.
[10] Y.J. Xie, B. Yan, H.L. Xu, J. Chen, Q.X. Liu, Y.H. Deng, H.B. Zeng, Highly regenerable mussel-inspired Fe_3O_4@Polydopamine-Ag core–shell microspheres as catalyst and adsorbent for methylene blue removal, ACS Appl. Mater. Interfaces, 6 (2014) 8845–8852.
[11] S.H. Cho, S.W. Jung, S.W. Jeong, J.W. Bang, J.H. Park, Y.R. Park, S.J. Kim, Strategy for synthesizing quantum dot-layered double hydroxide nanocomposites and their enhanced photoluminescence and photostability, Langmuir, 29 (2012) 441–447.
[12] G. Abellán, C. Martí-Gastaldo, A. Ribera, E. Coronado, Hybrid materials based on magnetic layered double hydroxides: a molecular perspective, Acc. Chem. Res., 48 (2015) 1601–1611.
[13] M. Dadwhal, M. Sahimi, T.T. Tsotsis, Adsorption isotherms of arsenic on conditioned layered double hydroxides in the presence of various competing ions, Ind. Eng. Chem. Res., 50 (2011) 2220–2226.
[14] F. Song, X. Hu, Exfoliation of layered double hydroxides for enhanced oxygen evolution catalysis, Nat. Commun., 5 (2014) 4477.
[15] G.L. Fan, F. Li, D.G. Evans, X. Duan, Catalytic applications of layered double hydroxides: recent advances and perspectives, Chem. Soc. Rev., 43 (2014) 7040–7066.
[16] F.L. Theiss, G.A. Ayoko, R.L. Frost, Synthesis of layered double hydroxides containing Mg^{2+}, Zn^{2+}, Ca^{2+} and Al^{3+} layer cations by co-precipitation methods—a review, Appl. Surf. Sci., 383 (2016) 200–2013.
[17] X.-L. Wu, L. Wang, C.-L. Chen, A.-W. Xu, X.-K. Wang, Water-dispersible magnetite-graphene-LDH composites for efficient arsenate removal, J. Mater. Chem., 21 (2011) 17353–17359.
[18] Z.Y. Sun, L.H. Gu, J.Y. Zheng, J.W. Zhang, L. Wang, F.L. Xu, C.G. Lin, A controlled release strategy of antifouling agent in coating based on intercalated layered double hydroxides, Mater. Lett., 172 (2016) 105–108.
[19] F. Song, X. Hu, Ultrathin cobalt–manganese layered double hydroxide is an efficient oxygen evolution catalyst, J. Am. Chem. Soc., 136 (2014) 16481–16484.

[20] C. Li, M. Wei, D.G. Evans, X. Duan, Layered double hydroxide-based nanomaterials as highly efficient catalysts and adsorbents, Small, 10 (2014) 4469–4486.
[21] W. Yao, S.J. Yu, J. Wang, Y.D. Zou, S.S. Lu, Y.J. Ai, N.S. Alharbi, A. Alsaedi, T. Hayat, X.K. Wang, Enhanced removal of methyl orange on calcined glycerol-modified nanocrystallined Mg/Al layered double hydroxides, Chem. Eng. J., 307 (2017) 476–486.
[22] F. Kovanda, T. Grygar, V. Dorničák, Thermal behaviour of Ni-Mn layered double hydroxide and characterization of formed oxides, Solid State Sci., 5 (2003) 1019–1026.
[23] T. Hibino, H. Ohya, Synthesis of crystalline layered double hydroxides: precipitation by using urea hydrolysis and subsequent hydrothermal reactions in aqueous solutions, Appl. Clay Sci., 45 (2009) 123–132.
[24] S.P. Paredes, G. Fetter, P. Bosch, S. Bulbulian, Sol–gel synthesis of hydrotalcite-like compounds, J. Mater. Sci., 41 (2006) 3377–3382.
[25] P. Benito, I. Guinea, F.M. Labajos, V. Rives, Microwave-assisted reconstruction of Ni, Al hydrotalcite-like compounds, J. Solid State Chem., 181 (2008) 987–996.
[26] F.M. Labajos, V. Rives, M.A. Ulibarri, Effect of hydrothermal and thermal treatments on the physicochemical properties of Mg–Al hydrotalcite-like materials, J. Mater. Sci., 27 (1992) 1546–1552.
[27] M.J. Climent, A. Corma, S. Iborra, K. Epping, A. Velty, Increasing the basicity and catalytic activity of hydrotalcites by different synthesis procedures, J. Catal., 225 (2004) 316–326.
[28] R.X. Sun, Y.P. Lu, K.Z. Chen, Preparation and characterization of hollow hydroxyapatite microspheres by spray drying method, Mater. Sci. Eng., C, 29 (2009) 1088–1092.
[29] A. Fahami, G.W. Beall, S. Enayatpour, F. Tavangarian, M. Fahami, Rapid preparation of nano hexagonal-shaped hydrocalumite via one-pot mechanochemistry method, Appl. Clay Sci., 136 (2017) 90–95.
[30] P. Benito, F.M. Labajos, L. Mafra, J. Rocha, V. Rives, Carboxylate-intercalated layered double hydroxides aged under microwave-hydrothermal treatment, J. Solid State Chem., 182 (2009) 18–26.
[31] L. Wang, B. Li, C. Chen, L. Jia, Structural characterization and related properties of the stearate anions intercalated Ni-Al hydrotalcite-like compound prepared by the microwave crystallization, J. Alloys Compd., 508 (2010) 426–432.
[32] M. Herrero, P. Benito, F.M. Labajos, V. Rives, Stabilization of Co^{2+} in layered double hydroxides (LDHs) by microwave-assisted ageing, J. Solid State Chem., 180 (2007) 873–884.
[33] R. Pourfaraj, S.J. Fatemi, S.Y. Kazemi, P. Biparv, Synthesis of hexagonal mesoporous MgAl LDH nanoplatelets adsorbent for the effective adsorption of Brilliant Yellow, J. Colloid Interface Sci., 508 (2017) 65–74.
[34] R. Marangoni, M. Bouhent, C. Taviot-Gueho, F. Wypych, F. Lerouxc, Zn_2Al layered double hydroxides intercalated and adsorbed with anionic blue dyes: a physico-chemical characterization, J. Colloid Interface Sci., 333 (2009) 120–127.
[35] Z.M. Ni, S.J. Xia, L.G. Wang, F.F. Xing, G.X. Pan, Treatment of methyl orange by calcined layered double hydroxides in aqueous solution: adsorption property and kinetic studies, J. Colloid Interface. Sci., 316 (2007) 284–291.
[36] T. Yan, R.Y. Li, Z.J. Li, J.K. Liu, G.L. Wang, Z.Q. Gu, A free template strategy for the fabrication of nickel/cobalt double hydroxide microspheres with tunable nanostructure and morphology for high performance supercapacitors, RSC Adv., 3 (2013) 19416–19422.
[37] S. Elbasuney, Surface engineering of layered double hydroxide (LDH) nanoparticles for polymer flame retardancy, Powder Technol., 277 (2015) 63–73.
[38] S. Özgümüs, M.K. Gök, A. Bal, G. Güçlü, Study on novel exfoliated polyampholyte nanocomposite hydrogels based on acrylic monomers and Mg–Al–Cl layered double hydroxide: synthesis and characterization, Chem. Eng. J., 223 (2013) 277–286.
[39] X.M. Lu, L.M. Meng, H.P. Li, N. Du, R.J. Zhang, W.G. Hou, Facile fabrication of ibuprofen–LDH nanohybrids via a delamination/reassembling process, Mater. Res. Bull., 48 (2013) 1512–1517.
[40] R.J. Qi, Y.J. Zhu, Microwave-assisted synthesis of calcium carbonate (Vaterite) of various morphologies in water-ethylene glycol mixed solvents, J. Phys. Chem. B, 110 (2006) 8302–8306.
[41] S. Mallakpour, M. Dinari, V. Behranvand, Ultrasonic-assisted synthesis and characterization of layered double hydroxides intercalated with bioactive N,N′-(pyromellitoyl)-bis-L-α-amino acids, RSC Adv., 3 (2013) 23303–23308.
[42] Q. Liu, B. Wang, C. Wang, Z. Tian, W. Qu, H. Ma, R. Xu, Basicities and transesterification activities of Zn–Al hydrotalcites-derived solid bases. Green Chem., 16 (2014) 2604–2613.
[43] S. Mallakpour, M. Dinari, M. Hatami, Modification of Mg/Al-layered double hydroxide with L-aspartic acid containing dicarboxylic acid and its application in the enhancement of the thermal stability of chiral poly(amide-imide), RSC Adv., 4 (2014) 42114–42121.
[44] L. Yang, Z. Shahrivari, P.K.T. Liu, M. Sahimi, T.T. Tsotsis, Removal of trace levels of Arsenic and Selenium from aqueous solutions by calcined and uncalcined layered double hydroxides (LDH), Ind. Eng. Chem. Res., 44 (2005) 6804–6815.
[45] H.J. Hu, J.Y. Liu, Z.H. Xu, L.Y. Zhang, B. Cheng, W.K. Ho, Hierarchical porous Ni/Co-LDH hollow dodecahedron with excellent adsorption property for Congo red and Cr(VI) ions, Appl. Surf. Sci., 478 (2019) 981–990.
[46] C.S. Lei, M. Pi, B. Cheng, C.J. Jiang, J.Q. Qin, Fabrication of hierarchical porous ZnO/NiO hollow microspheres for adsorptive removal of Congo red, Appl. Surf. Sci., 435 (2018) 1002–1010.
[47] S. Ghorai, A. Sarkar, M. Raoufi, A.B. Panda, H. Schönherr, S. Pal, Enhanced removal of methylene blue and methyl violet dyes from aqueous solution using a nanocomposite of hydrolyzed polyacrylamide grafted xanthan gum and incorporated nano-silica, ACS Appl. Mater. Interfaces, 6 (2014) 4766–4777.
[48] M. Liu, J. Xu, B. Cheng, W. Ho, J. Yu, Synthesis and adsorption performance of $Mg(OH)_2$ hexagonal nanosheet graphene oxide composites, Appl. Surf. Sci., 332 (2015) 121–129.
[49] X. Wu, W. Wang, F. Li, S. Khaimanov, N. Tsidaeva, M. Lahoubi, PEG-assisted hydrothermal synthesis of $CoFe_2O_4$ nanoparticles with enhanced selective adsorption properties for different dyes, Appl. Surf. Sci., 389 (2016) 1003–1011.
[50] P. Tian, X.Y. Han, G.L. Ning, H.X. Fang, J.W. Ye, W.T. Gong, Y. Lin, Synthesis of porous hierarchical MgO and its superb adsorption properties, ACS Appl. Mater. Interfaces, 5 (2013) 12411–12418.
[51] T. Maneerung, J. Liew, Y.J. Dai, S. Kawi, C. Chong, C.H. Wang, Activated carbon derived from carbon residue from biomass gasification and its application for dye adsorption: kinetics, isotherms and thermodynamic studies, Bioresour. Technol., 200 (2016) 350–359.
[52] J. Zhao, Q. Huang, M.Y. Liu, Y.F. Dai, J.Y. Chen, H.Y. Huang, Y.Q. Wen, X.L. Zhu, X.Y. Zhang, Y. Wei, Synthesis of functionalized MgAl-layered double hydroxides via modified mussel inspired chemistry and their application in organic dye adsorption, J. Colloid Interface Sci., 505 (2017) 168–177.
[53] S. Ghorai, A.K. Sarkar, A.B. Panda, S. Pal, Effective removal of Congo red dye from aqueous solution using modified xanthan gum/silica hybrid nanocomposite as adsorbent, Bioresour. Technol., 144 (2013) 485–491.